Schneider et al., http://www.jcb.org/cgi/content/full/jcb.201307088/DC1

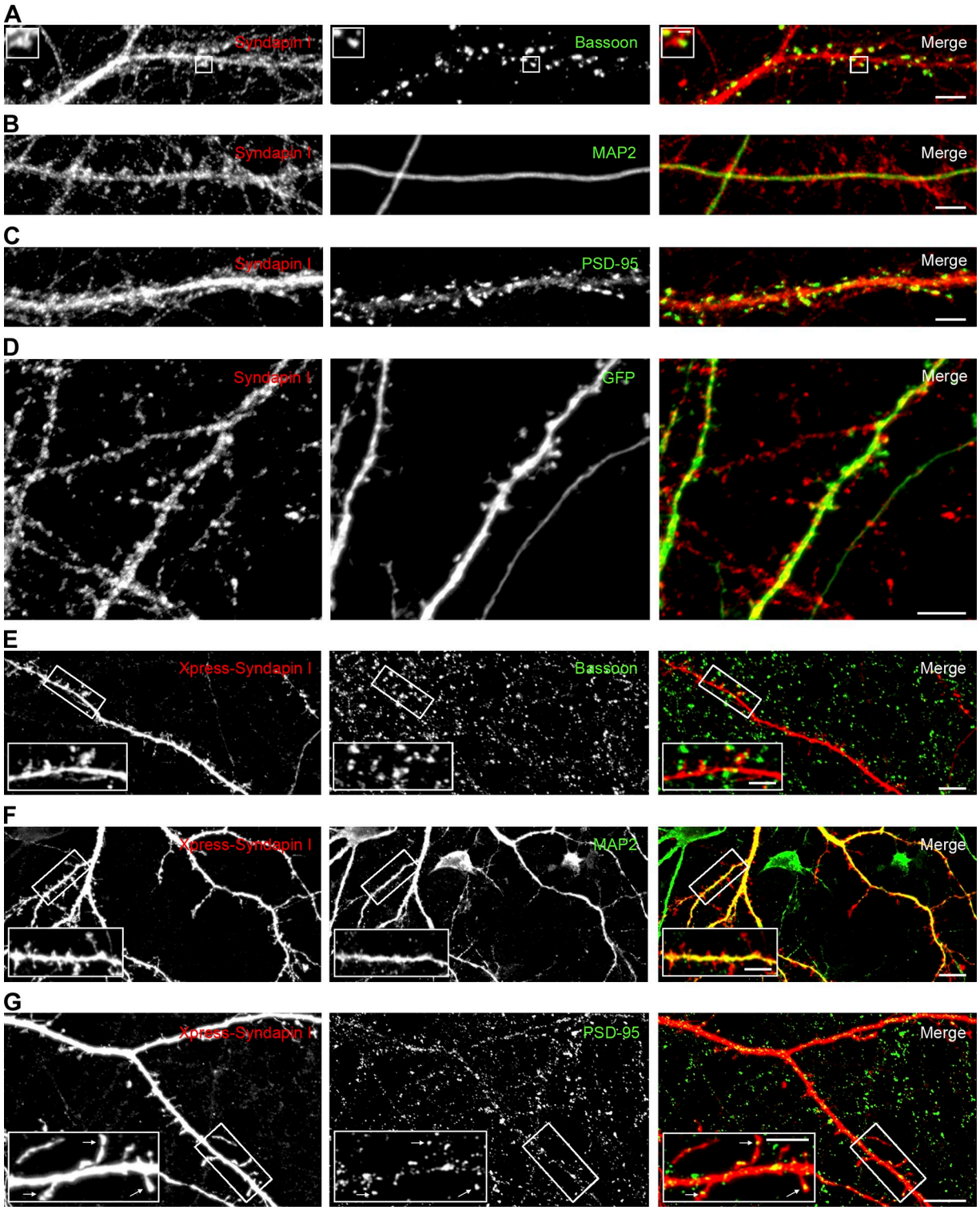

Figure S1. **Syndapin I is present in both the axonal/presynaptic as well as the dendritic/postsynaptic compartment.** (A–C) Coimmunolabeling of endogenous syndapin I and markers for the presynaptic (A), dendritic (B), and postsynaptic (C) compartment of primary hippocampal neurons, respectively. Overlap of anti–syndapin I with anti-Bassoon, anti-MAP2, and anti–PSD-95 immunolabeling shows syndapin I localizations in dendrites and synapses of mature primary hippocampal neurons (DIV 21). (D) Transfection with GFP (at DIV 12) as cell filler highlighting the complete morphological features of primary hippocampal neurons (DIV 14) also demonstrates that a significant portion of anti–syndapin I immunolabeling is present in dendrites and spines. (E–G) Localization of Xpress-tagged syndapin I and markers for the presynaptic, dendritic, and postsynaptic compartments of primary hippocampal neurons at DIV 14. (E) Bassoon colabeling shows that presynapses contact Xpress–syndapin I–positive dendritic protrusions of transfected cells. (F) MAP2 staining demonstrates that syndapin I–containing spiny protrusions arise from the dendrites of transfected cells. (G) The heads of syndapin I–costained spiny protrusions are anti–PSD-95 positive (arrows in insets). Insets are twofold enlargements of the boxed areas. Syndapin I is shown in red, marker/GFP in green in the merged images. Bars: (A–D) 5 µm; (A, inset) 2 µm; (E–G) 10 µm; (E–G, insets) 5 µm.

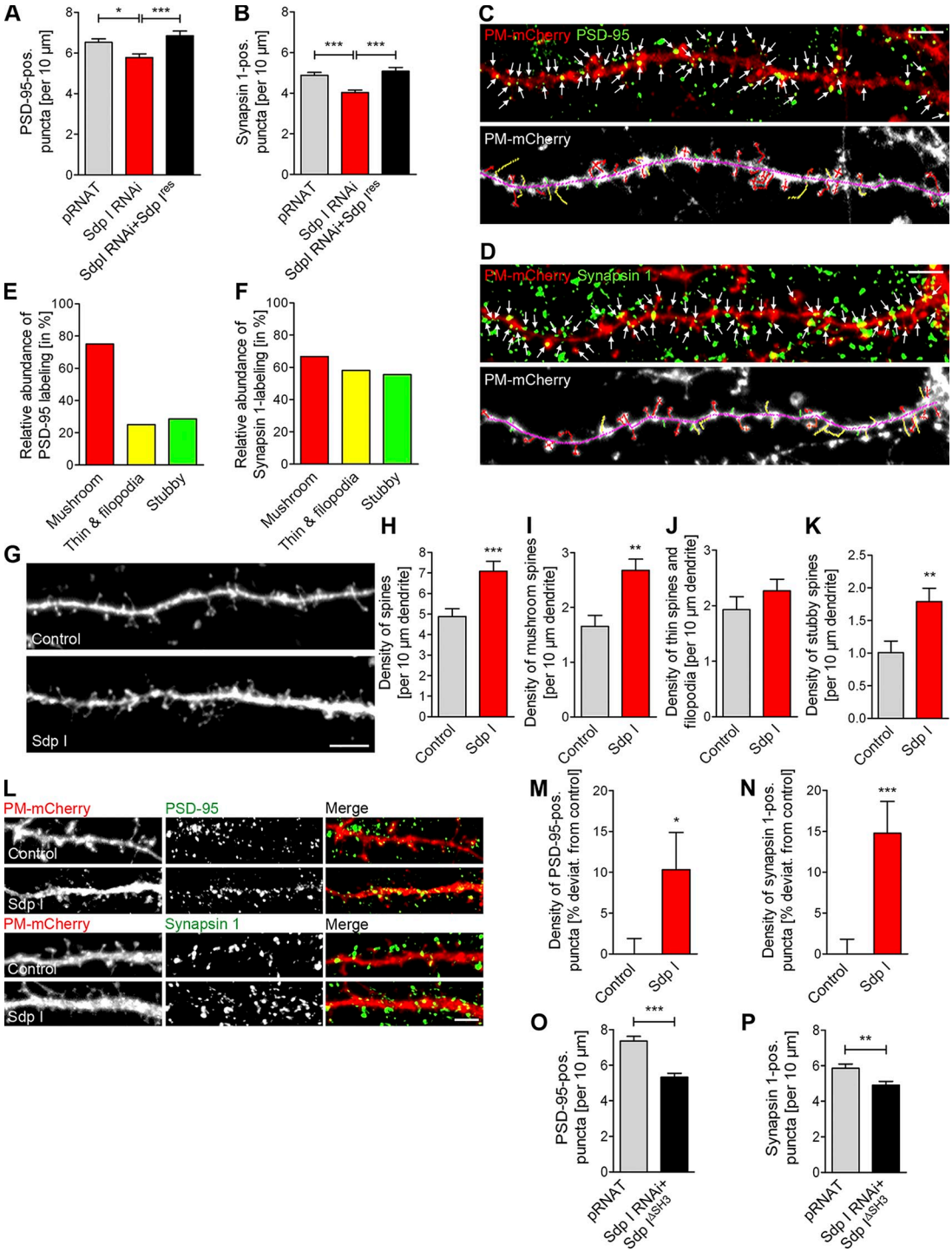

Figure S2. **Syndapin I RNAi decreases the density of synapses, whereas syndapin I overexpression increases the density of mushroom spines and synapses.** (A and B) Absolute values of densities of PSD-95– and synapsin 1–positive puncta along dendrites of neurons transfected as indicated (compare with Fig. 2 [E–G] for normalized data). (A) pRNAT, *n* = 196; Sdp I RNAi, *n* = 210; Sdp I RNAi+Sdp I^{res}, *n* = 164 dendrite sections. (B) pRNAT, *n* = 186; Sdp I RNAi, *n* = 219 dendrite sections; Sdp I RNAi+Sdp I^{res}, *n* = 181; one-way ANOVA with Tukey's post test. (C and D) Representative images of synapse density (top) and spine morphology analysis (bottom) of neurons expressing PM-mCherry fixed at DIV 14 and stained for PSD-95 (C) and synapsin 1 (D). (E) Comparison of the analysis of PSD-95 puncta (marked by arrows in C) with spine morphology analysis demonstrates that the majority of mushroom spines are PSD-95 positive. (F) Analysis of synapsin 1–positive puncta at/in close conjunction with the dendrite or spines (marked by arrows in D) compared with the spine morphology analysis shows that the majority of analyzed spines are contacted by presynapses. Spine morphology groups are marked in the bottom panels of C and D according to color code used in E and F. (G) Images of dendrite sections of primary hippocampal neurons (transfected at DIV 12 and fixed after 2 d) illustrating the increased spine density, especially of mushroom-type spines, upon syndapin I overexpression. PM-mCherry fluorescence (presented) was used to evaluate neuronal morphologies. (H–K) Quantification of general spine density (H) and of individual morphology groups (I, mushroom spines; J, thin spines and filopodia; K, stubby spines) of neurons transfected with PM-mCherry alone (control) and cotransfected with syndapin I, respectively. (H–K) Control, *n* = 19; Sdp I, *n* = 16 dendrite sections. (L) Representative images of immunolabelings with anti–PSD-95 (postsynaptic marker) and anti–synapsin 1 (presynaptic marker) antibodies of neurons overexpressing syndapin I together with PM-mCherry (morphology tracer) show an increase in synapse densities compared with control cells. PM-mCherry is shown in red, marker in green the merged images. (M and N) Quantitative evaluation of the number of PSD-95– and synapsin 1–positive puncta on dendrites of transfected neurons normalized to control. (M) Control, *n* = 196; Sdp I, *n* = 80. (N) Control, *n* = 186; Sdp I, *n* = 67 dendrite sections. (O and P) Absolute numbers of the densities of PSD-95– and synapsin 1–positive puncta along dendrites of neurons coexpressing syndapin I RNAi and an RNAi-insensitive syndapin I ΔSH3 mutant (Sdp $I^{\Delta SH3}$; compare with Fig. 2 [E–G] for normalized data). (O) pRNAT, *n* = 71; Sdp I RNAi+Sdp $I^{\Delta SH3}$, *n* = 71. (P) pRNAT, *n* = 57; Sdp I RNAi+Sdp $I^{\Delta SH3}$, *n* = 84 dendrite sections. (H–K and M–P) Unpaired, two-tailed Student's t-test. *, P < 0.05; **, P < 0.01; ***, P < 0.001. Data represent mean ± SEM (error bars). Bars, 5 µm.

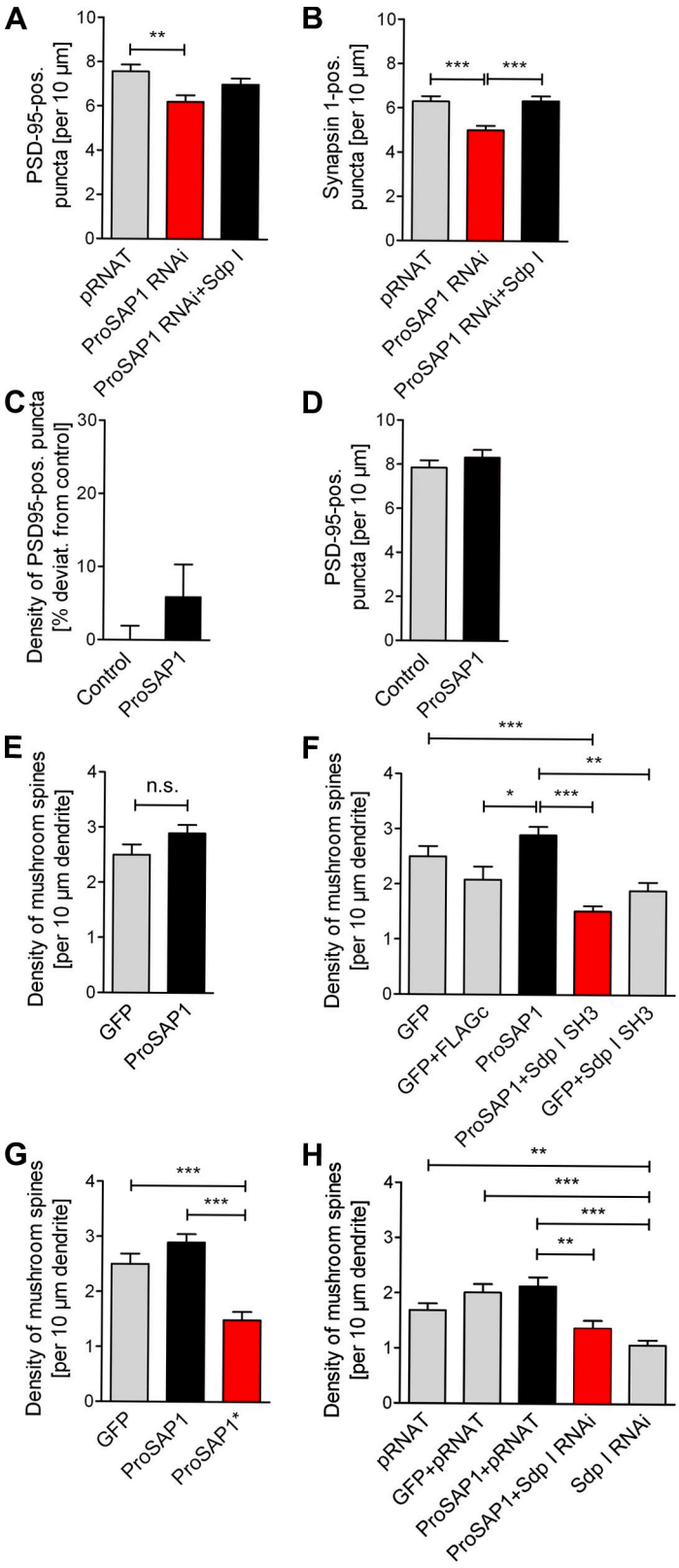

Figure S3. **Syndapin I and ProSAP1 cooperate in spine and synapse formation.** (A and B) Quantification of PSD-95– (A) and synapsin 1–positive puncta densities (B) in absolute numbers (compare with Fig. 6 [B and C] for data normalized to controls run in parallel). (A) pRNAT, *n* = 69; ProSAP1 RNAi, *n* = 86; ProSAP1 RNAi+Sdp I, *n* = 77. (B) pRNAT, *n* = 64; ProSAP1 RNAi, *n* = 69; ProSAP1 RNAi+Sdp I, *n* = 85 dendrite sections. One-way ANOVA with Tukey's post test. (C and D) Quantitative evaluation of the number of PSD-95– and synapsin 1–positive puncta on dendrites of transfected neurons normalized to control (C) and in absolute numbers (D). (C) Control, *n* = 196; ProSAP1, *n* = 45. (D) Control, *n* = 54; ProSAP1, *n* = 45 dendrite sections; unpaired, two-tailed Student's *t* test (both not significantly different). (E–H) Quantitative examination of mushroom spine density. (E) GFP, *n* = 20; ProSAP1, *n* = 23. (F) GFP, *n* = 20; GFP+FLAGc, *n* = 11; ProSAP1, *n* = 23; ProSAP1+Sdp I SH3, *n* = 16; GFP+Sdp I SH3, *n* = 11. (G) GFP, *n* = 20; ProSAP1, *n* = 23; ProSAP1*, *n* = 14. (H) pRNAT, *n* = 23; GFP+pRNAT, *n* = 8; ProSAP1+pRNAT, *n* = 15; ProSAP1+Sdp I RNAi, *n* = 19; Sdp I RNAi, *n* = 22 dendrite sections; one-way ANOVA with Tukey's post test. *, P < 0.05; **, P < 0.01; ***, P < 0.001. Data represent mean ± SEM (error bars).

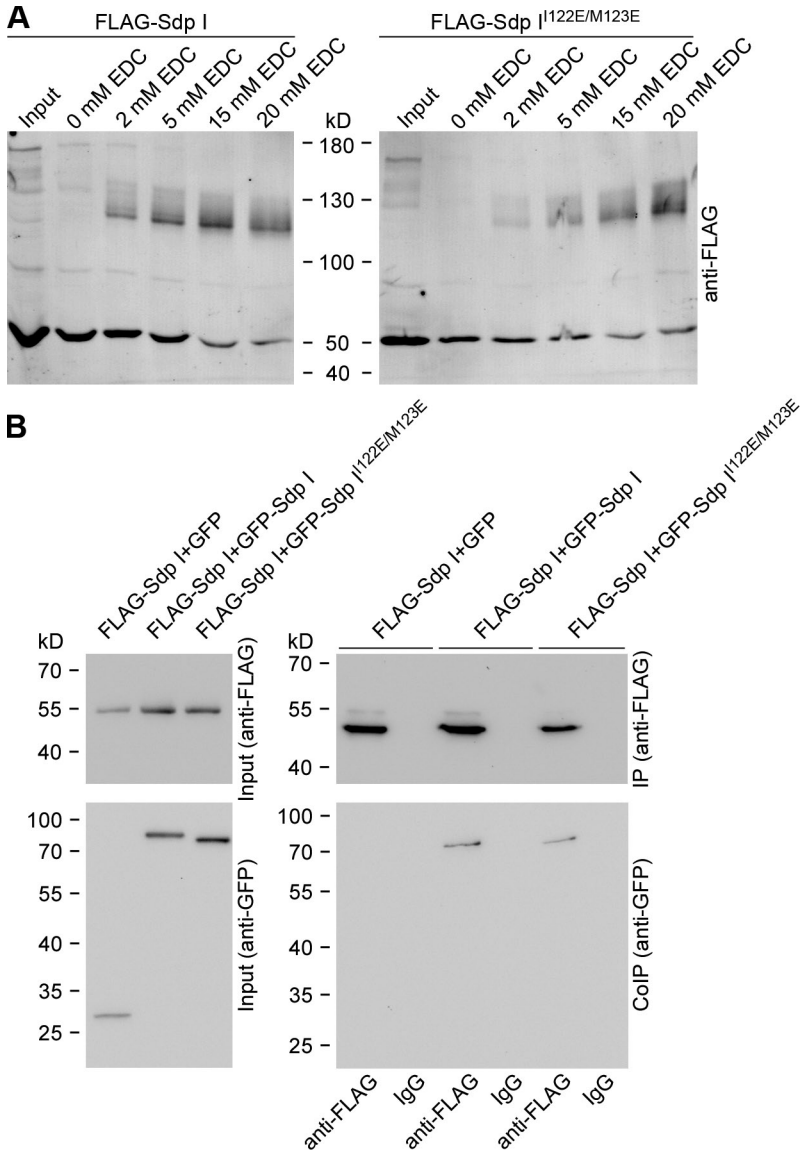

Figure S4. **I122E and M123E mutation in the syndapin I wedge loop does not affect syndapin I self-association.** (A) Immunoblot analyses of lysates from HEK293 cells expressing WT and wedge loop mutant FLAG–syndapin I (Sdp I$^{I122E/M123E}$), which were incubated with varying amounts of the cross-linker EDC. EDC incubation leads to an EDC concentration–dependent appearance of a band with twice the molecular weight of syndapin I (~100 kD) and a reduction in the syndapin I monomer signal (~50 kD) for both WT syndapin I and syndapin I$^{I122E/M123E}$. (B) Heterologous coimmunoprecipitation of GFP–syndapin I and of GFP–syndapin I$^{I122E/M123E}$, respectively, with FLAG-tagged syndapin I coexpressed in HEK293 cells. Immunoblot analyses show that mutation in the wedge loop of syndapin I does not impair coimmunoprecipitation compared with WT syndapin I.

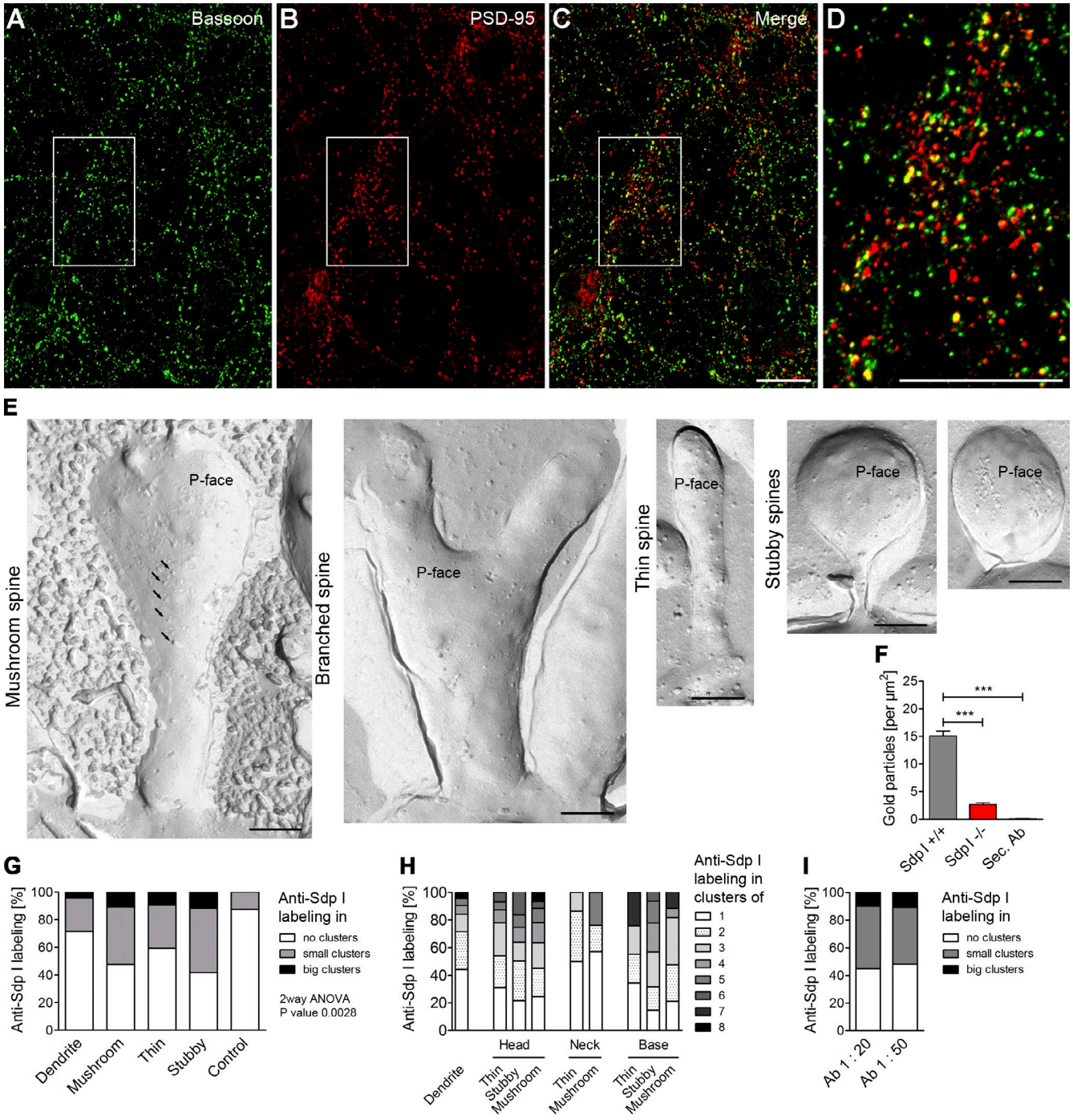

Figure S5. **Freeze-fracturing of hippocampal neurons and quantitative analysis of syndapin I nanodomains.** (A–D) Primary hippocampal neurons on sapphire discs form normal networks with synaptic contacts. Primary hippocampal neurons were grown for 16 d on poly-L-lysine–coated sapphire discs, fixed, and subjected to anti-Bassoon (A) and anti–PSD-95 (B) immunolabeling. (C) Merged image (colocalization appears yellow). (D) Threefold enlargement of the boxed area in C. Bars, 10 µm. (E) Examples of dendritic spines preserved in freeze-fractured primary hippocampal neurons. Shown is a gallery of electron micrographs of freeze-fracture replica of hippocampal neurons at DIV 16 showing different types of dendritic spines with fully preserved morphology. Note that filopodia were not observable in freeze-fractured neurons at DIV 16. Compiled are images of mushroom, branched, thin, and stubby spines. P-faces contain abundant integral membrane protein complexes (a few examples are marked by arrows at the mushroom spine membrane). Bars, 200 nm. (F) Anti–syndapin I labeling at freeze-fractured membranes of spines is specific, as shown by quantitative analyses of labeling densities obtained in the secondary antibody control (Sec. Ab) and in parallel incubations of syndapin I KO replica with anti–syndapin I and gold-conjugated secondary antibodies (Sdp I−/−) in comparison to anti–syndapin I immunogold labeling at freeze-fractured brain material from WT mice (Sdp I +/+). n = 20 spines each. ***, $P < 0.001$. Data represent mean ± SEM (error bars). (G and H) Simplified (G) and detailed (H) quantitative analysis of anti–syndapin I labeling clusters at membranes of different spine classes and different membrane areas of dendritic spines. Shown are the percentages of single and clustered anti–syndapin I immunogold labeling at indicated membrane areas of spines of the indicated type. Maximal cluster size was restricted to 100 nm. Note that spine neck regions are similar to dendrite areas and are marked by single and double labelings, whereas spine head regions as well as spine bases are marked by clusters of membrane-associated syndapin I. (I) Changes in anti–syndapin I antibody concentrations did not alter the clustered anti–syndapin I immunogold labeling in spines (all classes). 1:20 dilution of antibody (Ab 1:20), n = 32 spines; Ab 1:50, n = 134 spines. Two-way ANOVA, not significantly different.